Nuclear Instruments and Methods in Physics Research A 620 (2010) 83–87

Contents lists available at ScienceDirect

Nuclear Instruments and Methods in Physics Research A

journal homepage: www.elsevier.com/locate/nima

Laser-accelerated ions from layered targets

L.A. Gizzi [a,b,*], S. Betti [a,b,1], E. Förster [c], A. Giulietti [a,b], D. Giulietti [a,b,d], T. Kämpfer [c], P. Köster [a,b], L. Labate [a,b], T. Levato [a,b], A. Lübcke [c,2], A.P.L. Robinson [e], I. Uschmann [c], F. Zamponi [c,2]

[a] ILIL, Istituto Nazionale di Ottica, CNR Campus, Via G. Moruzzi, 1 - 56124 Pisa, Italy
[b] INFN, Sezione di Pisa, Largo B. Pontecorvo 3, Pisa, Italy
[c] Insitut für Optik und Quantenelektronik - Friedrich-Schiller-Universität, Max-Wien-Platz 1, 07743 Jena, Germany
[d] Dipartimento di Fisica, Università degli Studi, Pisa, Italy
[e] Central Laser Facility, Rutherford Appleton Laboratory, Chilton, OX11 0QX, UK

ARTICLE INFO

Available online 10 February 2010

Keywords:
Ion acceleration
Proton acceleration
High energy bunches
Laser-plasma acceleration
Laser-driven bunches
Numerical simulations
PIC

ABSTRACT

We investigated laser-driven ion acceleration with tightly focused femtosecond laser pulses at an intensity of 5×10^{19} W/cm^2. Targets consisting of thin metal foils either back-coated with a μm−thick dielectric layer or uncoated have been used. The observations we report show that proton bunches with energy in the MeV range have been produced. Furthermore, the protons emitted from back-coated targets exhibit a spatial cross-section which is remarkably more uniform and of significantly smaller size if compared with that of the protons emitted from uncoated foils. The experimental results are discussed in terms of the differences between the propagation of the fast electron current inside the back-coated and uncoated targets.

1. Introduction

Laser-driven ion acceleration has, in the past 10 years, gained considerable attention [1–13] because of the extremely diversified and relevant applications in which high energy ion beams can play a significant role, among which hadron therapy [14–22], inertial confinement fusion (ICF) [23,24] and proton imaging [25–27] are worth mentioning. All-optical accelerators are nowadays considered a promising opportunity because of the extremely low emittance (<0.004 mm rad), the small divergence ($\approx10^\circ$) and the high values of the currents (>1 kA) typically characterizing the laser-accelerated ion bunches [28,29], together with the potentially smaller size of such particle accelerators if compared with the conventional ones. Nevertheless, laser-driven ion acceleration has recently become even more attractive since table-top, high-repetition rate laser systems can now be used in place of large, single-shot systems.

After the pioneering experiments demonstrating emission of protons from the rear target surface [30], further experimental work clarified the role played by the prepulse [31], and recently, laser-driven acceleration has also been efficiently achieved with femtosecond, high contrast laser systems and with the employment of ultrathin foils [32]. Furthermore, a significant reduction of the relative energy spread has been obtained using custom targets [33–35].

At present, special effort is devoted to improve the quality of these laser-accelerated bunches, in particular for what regards the spectral and angular features, the total ion yield and the spatial cross-section uniformity. In fact, the production of laser-accelerated ion bunches of high quality represents a major progress, in particular for applications like advanced probing [36], or in view of an efficient extraction, transport and focusing of the laser accelerated ions in an user-oriented set-up [37].

For such purposes, recent theoretical and experimental efforts have shown that double-layer targets [16] might be fruitfully adopted in order to achieve a systematic control of the quality of laser-driven ion bunches [38,39]. In particular, from an experimental point of view, the use of target back-surface coatings resulted, in the picosecond regime, in a significant increase of the accelerated protons yield [40]. Such beneficial effect on proton acceleration has more recently been experimentally confirmed also in the femtosecond regime, where the employment of double-layer targets again allowed to strongly increase the protons yield [41,42].

However, apart from the aforementioned beneficial effects, experimental studies [43] have also revealed that the presence of plastic coatings may have a strong detrimental effect on the uniformity of the spatial cross-section of the accelerated ions. Such an effect has been observed for plastic coatings thicker than

* Corresponding author at: ILIL, Istituto Nazionale di Ottica, CNR Campus, Via G. Moruzzi, 1 - 56124 Pisa, Italy.
E-mail address: leonidaantonio.gizzi@ino.it (L.A. Gizzi).
[1] Also at Accademia Navale, Livorno, Italy, and at Dipartimento di Ingegneria delle Telecomunicazioni, Università degli Studi di Pisa, Italy.
[2] Current address: Max Born Institute, Berlin, Germany.

0168-9002/$ - see front matter © 2010 Elsevier B.V. All rights reserved.
doi:10.1016/j.nima.2010.01.065

0.1 μm [43,44], and has been attributed to a disruption of the fast electron current which, in many experiments, has been observed to occur inside dielectric layers [45]. For such reasons, the laser–target coupling mechanisms giving rise to the fast electrons [46] on the irradiated foil surface together with the transport dynamics of the fast electron current occurring inside the target [47,48] have thus emerged as fundamental issues to be carefully addressed also in the study of laser-driven ion acceleration.

In the present paper, we show the results of an ion-acceleration experiment which has been carried out using a table-top, femtosecond laser system and which was aimed at exploring the role of dielectric back-surface coatings in ion acceleration. In our experiment, laser-accelerated proton bunches with energy of some MeV were obtained by irradiation of targets either uncoated or back-coated with a μm−thick dielectric layer. Our measurements gave results [50] that are in contrast with those reported in Refs. [43,44]. In fact, proton bunches with systematically more uniform cross-sections were obtained from back-coated foils.

In the following we show measurements of both the energy and the spatial cross-section of a proton bunch which is typically obtained, under our experimental conditions, after irradiation of a metal foil *with* and *without* the rear-surface plastic coating. The comparison we will present shows that the spatial cross-section from coated targets is of a significantly smaller size and much more uniform than that from uncoated targets. To our knowledge, this is the first experimental evidence that, in spite of previous observations, dielectric coatings may be used to add control on laser-accelerated proton bunches by reducing the overall size and increasing the uniformity of their spatial cross-sections. As discussed below, since proton acceleration is inherently linked with fast electron transport processes, the results presented here are being modeled looking at the transport dynamics of the fast electron current occurring inside back-coated targets. Here we will give a preliminary account of the modeling approach and the physical processes taken into account.

The paper is organized as follows. In Section 2 we describe the experimental setup adopted. Section 3 is dedicated to showing the results obtained regarding ion acceleration in both back-coated and uncoated targets, which are then discussed in Section 4. Finally, Section 5 is devoted to present our conclusions.

2. Experimental setup

A sketch of the experimental setup adopted is shown in Fig. 1. We used an $f/1.2$ off-axis parabola to focus, with an angle of incidence of 10° on the target surface, 80 fs, 600 mJ laser pulses into 5 μm^2 diameter focal spots. The average intensity available on target was up to 5×10^{19} W/cm^2, with an intensity contrast ratio of 10^{10} between the amplified spontaneous emission and the main pulse [49]. The corresponding normalized vector potential was $a_0 = eA_L/m_ec^2 \approx 0.85\lambda_0\sqrt{I_L} = 4.8$, with e and m_e the electron charge and mass, A_L the laser vector potential, c the speed of light, λ_0 the laser wavelength in μm and I_L the intensity in units of 10^{18} W/cm^2, respectively.

The targets employed here are either 10 μm−thick, rear-surface coated Fe foils or 5.7 μm−thick, uncoated Ti foils. The coating adopted, being a nitrocellulose lacquer, can be regarded as a material characterized by a high content of light elements like H and C (e.g. $C_6H_7(NO_2)_3O_5$). The thickness of the coating has been measured to be 1.5 μm, while its resistivity has been found to be greater than 1.5×10^7 Ω/m. Due to the properties of lacquers, the coating adopted here should be regarded as a dielectric layer characterized by hardness, flexibility and a high adhesion to the substrate.

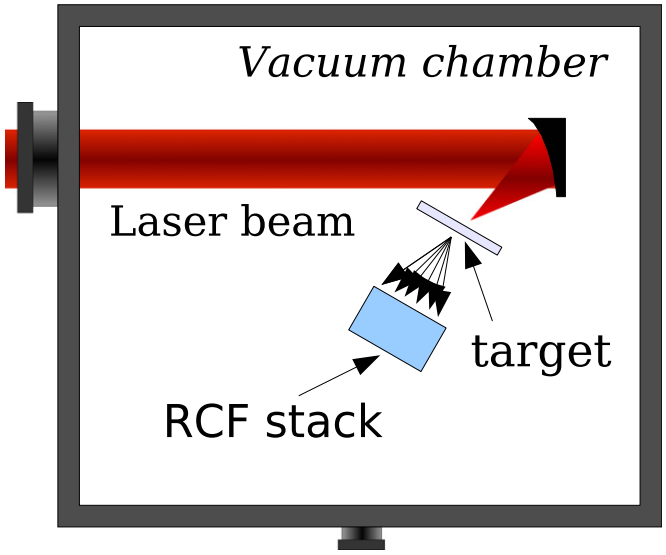

Fig. 1. Schematic layout of the experimental setup showing the laser pulse, the target position and the radiochromic film stack behind the target.

Particles have been detected by employing radiochromic films (RCF), which have been stacked behind the target at a distance of 7 mm and shielded from direct laser radiation by a 20 μm thick Al foil. The RCF response has been fully characterized [51] using Monte Carlo simulations based upon the numerical code GEANT4 [52]. As discussed in detail in Refs. [48,53,54], our dosimetric measurements also enable us to obtain information regarding the spatial uniformity, the energy and angular distribution of the forward-propagating fast electrons which escape from the target back surface with energy between about 100 keV and several MeV, together with an estimate of the total number of fast electrons in the detected spectral range.

3. Experimental results

3.1. Spatial features

Fig. 2 (left) shows the optical density scan of the first (HD810) RCF layer of the stack after irradiation of a back-surface coated target. The image shows a main ion signal superimposed on a smooth electron background, the latter being visible on the entire exposed area of the RCF.

The ion pattern consists of a regular, almost circular, uniform region, whose baseline level size is 4.3 mm in diameter. The high spatial uniformity and the step-like profile feature of the ion bunch spatial cross-section can be seen also in the three dimensional plot of Fig. 2. In contrast, we found a completely different scenario when we irradiated uncoated targets.

The ion bunch image visible in Fig. 3 shows the optical density scan of the first RCF layer of the stack after irradiation of a 5.7 μm thick, uncoated, Ti foil target. The ion signal is now characterized by an irregularly shaped, hot-spotted pattern with an overall size, i.e. the area containing the entire ion signal, being almost four times the size of the pattern of Fig. 2 along the vertical axis. The blank circle visible on the bottom-left corner of the image represents the size of the ion bunch of Fig. 2 and is reported here for comparison.

3.2. Proton beam energy

The signal was attributed to protons because of the more favourable charge-to-mass ratio of protons compared to other

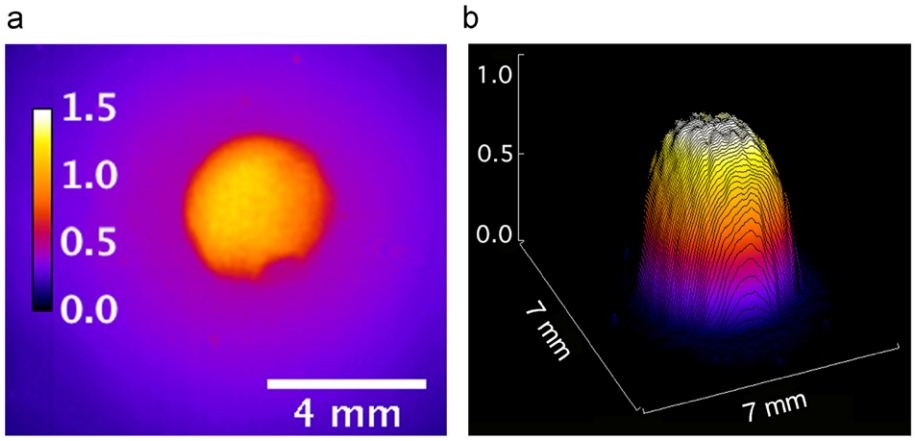

Fig. 2. False color image showing (left) the optical density of the first RCF layer after exposure in case of a back-surface coated, 10 μm thick Ti target. The ion signal, which consists of a regular, almost circular, uniform region is superimposed on a smooth electron background. The flatness of the ion bunch pattern is clearly visible in the 3D plot (right).

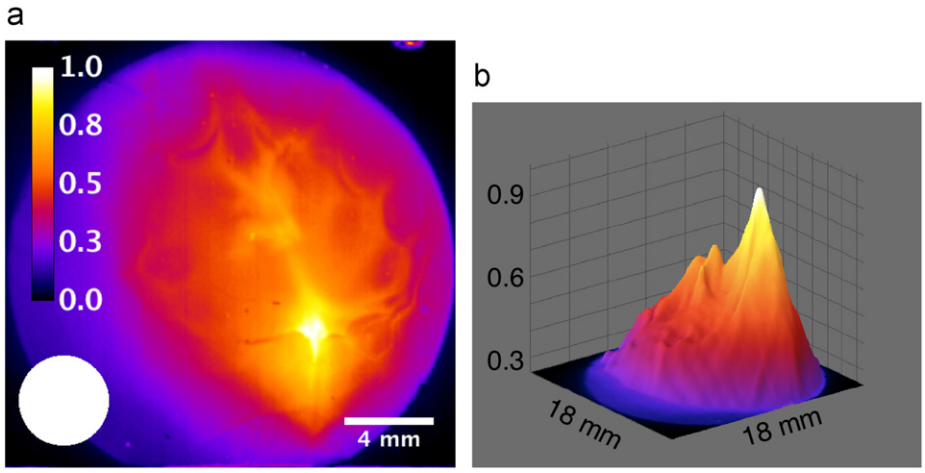

Fig. 3. Ion bunch after irradiation of an uncoated target. The false color image (left) shows the optical density of the first RCF layer after exposure. The blank circle on the bottom-left of the image shows, for comparison, the size of the ion bunch of Fig. 2. The strong non-uniformities of the ion bunch are clearly visible also in the 3D plot (right).

ions. In order to obtain information regarding their energy range we have carried out a proton radiography of a Ta grid consisting of 35 μm diameter Ta wire. The grid was placed in front of the RCF detector which was, in turn, shielded by a 20 μm thick Al foil. Therefore, taking into account that the protons were transmitted through the 20 μm thick Al foil placed in front of the RCF stack allowed us to estimate the lower limit to the proton energy which, by using the numerical code SRIM [55], was found to be $U_{\min} \approx 1.2$ MeV. The upper limit to the proton energy has been conversely inferred by observing that, as can be confirmed by a quantitative analysis of the radiography, the protons were not capable of penetrating the full diameter of a single Ta wire in addition to the Al foil. Therefore, according to additional calculations performed using the code SRIM, the upper value to the proton energy is found to be $U_{\max} \approx 3.6$ MeV.

As a preliminary step towards the understanding of the observed proton energy, we performed numerical, particle-in-cell (PIC), collisionless simulations [56]. The simulations are 3D in the particles velocities and 1D in the cartesian coordinates. The target is modeled as a fully ionized, quasineutral, Ti bulk plasma. A thinner layer of fully ionized, hydrogen plasma is added on the rear—i.e. the non-irradiated—side in order to model an hydrogen rich coating. The electron density profile, qualitatively sketched in Fig. 4, in 2 μm ramps up from zero to 110 n_c, with n_c the critical density which, for the 800 nm wavelength considered here, equals to $n_c \approx 1.74 \times 10^{21}$ cm^{-3}. This ramp in the electron density profile has been introduced in order to model the preplasma which is expected to be created by the laser prepulse. After the ramp the plasma density is constant for a length which is equal to the target thickness plus the contaminant layer thickness, and finally abruptly falls to zero in a step-like fashion. In both the preplasma and in the target region the electrons are locally neutralized by a fully ionized (Z=22, A=48) Ti background of density equal to five times the critical density. Furthermore, in the contaminant layer the electrons are locally neutralized by a proton background (Z=1, A=1) of density equal to that of the negatively charged particles. The laser is assumed to be Gaussian in time with a 70 fs pulse duration FWHM (full width at half maximum) and with a peak intensity of 5×10^{19} W/cm^2, and it impinges normally on the target side on which the plasma presents the density ramp, i.e. from left to right when referring to Fig. 4. In the model simulations the thickness of the Ti foil and of the contaminant layer were 5 μm and 20 nm, respectively.

According to our PIC simulations, we find that about 95% of the protons acquire an energy of about 4.4 MeV, consistently with the experimental value reported above of 3.6 MeV. In a similar way, we find that the maximum energy of the Ti ions we obtain from the simulations is $U_{i,M} \approx 60$ MeV. Therefore, as according to the numerical code SRIM the stopping range of 60 MeV ions in aluminum is roughly equal to 13 μm, which is definitely smaller

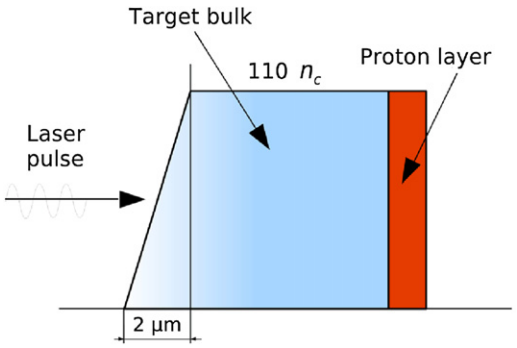

Fig. 4. Schematic diagram showing the main features of the electron density profile used in the PIC simulations.

than the thickness of the Al foil used in our experiment, we can be confident that the heavy particle signal observed on the RCF was not due to Ti ions.

4. Discussion

As a general consideration, we stress that the modeling of the observed experimental results is a very complex task that is beyond the possibilities of existing codes. Our approach here is to identify aspects of the entire physical process that can be addressed separately and focus our attention to those aspects that are more relevant in our experimental configuration. In fact, the role of fast electron generation processes at the laser–target interface is of a limited relevance here as fast electron generation will, most likely, not depend upon the presence of a target back-surface coating. Once fast electrons are generated, transport and energy deposition of these fast electrons will clearly depend dramatically upon the geometrical and physical properties of the material.

Based upon the target normal sheath acceleration (TNSA) scenario (see Refs. [10–13] and references therein), which can be expected to be a sound theoretical description of the experimental regime investigated here, ion acceleration is due to a strong electrostatic field that builds up when the fast electrons produced by the interaction of the laser pulse with the front surface propagate inside the foil and reach the back of the target.

In this scenario, additional experimental information on the properties of fast electrons is clearly of a crucial importance. To this purpose, we observe that measurements [48] of the forward escaping fast electrons were taken in the same experimental campaign. Those measurements, which gave information only on the high energy component of the fast electrons, provide no clear evidence of effects due to the presence of the rear side coating, suggesting that the effect of dielectric layer on the fast electron transport may be limited to the low energy part of the fast electrons. We stress, however, that our measurements on forward escaping fast electrons could not be resolved in angle, due to diffusion in the RCF stack. Therefore we can only speculate here that the reduction of the transverse size of the accelerated protons found in the case of rear-coated targets may be attributed to selection of fast electrons propagating on-axis through the dielectric layer.

Another important aspect regarding the comparison of our results with previous results obtained with back-surface coated targets is the role played by the specific target properties. Needless to say, the transport of the kA currents of fast electrons which are typical of such interaction conditions strongly depends on the conductivity of the medium, which must sustain the propagation by establishing a cold return current [57,58]. It has been shown that in the case of propagation in dielectric targets [59], these conditions are not fulfilled and inhibition of the fast electron transport occurs. The effect is even more pronounced in case the fast electron current propagates into low density materials, like gas targets [60] and low density foams [61] as the density of electrons available to establish return currents is low if compared to solids.

In the case of typical back-surface plastic coatings, vacuum gaps may be present between the substrate and the coating due to the poor adhesion of plastic layers obtained from vacuum deposition onto metal surfaces. Indeed, one may expect the quality of the interface to play a significant role in the transport of the fast electron current propagation in case of coated targets.

In our experiment we use, for the first time, a different type of dielectric coating which is different from standard plastic coatings from the point of view of adhesion to the substrate. The high adhesion of the lacquer employed here might have reduced or eliminated any vacuum gap with respect to standard coatings, resulting in an inhibition of the fast electron transport limited to the low energy component of the fast electron current only. This might thus qualitatively account for the differences between our observations and those reported in Ref. [43].

Based upon these considerations, in the case of back-surface coated targets, we can consider fast electron transport taking place in a two-layer configuration, where interface effects can be treated in a close to ideal condition.

The task is therefore to investigate the transport of the fast electrons in a dielectric coated metal target, in conditions similar to those occurring in our experiment. To this purpose we use a 2D hybrid Vlasov–Fokker–Planck (VFP) numerical code LEDA [62]. The code uses a KALOS-like [63] algorithm to describe the fast electrons, whilst the background electrons are given a hybrid description [64].

The distribution function of the fast electrons is expressed as a truncated spherical harmonic expansion with terms of the form $f_l^m(x,y,p)P_l^m(\cos\theta)\exp(im\phi)$. Substituting this expansion into the VFP equation yields a set of equations for the $f_l^m(x,y,p)$ coefficients. A brief description of the solution of these equations by means of the KALOS algorithm is given in Ref. [63].

This code was previously used in the work reported in Refs. [62,65], and has been extended to include the collisional drag on the fast electrons. The reflective boundaries are used in both x and y. For these simulations a box of 4800 cells in x and 40 cells in y were used, and a cell size of 0.2 μm was set in both x and y. Fast electrons were injected with an isotropic angular distribution from a region in the center of the bottom edge of the simulation box, i.e. the y-direction represents the thickness of the foil. This modeled a laser with a FWHM duration of 80 fs, an intensity of 5×10^{19} W/cm^2, and a FHWM spot diameter of 6 μm. The laser to fast electron energy conversion efficiency was set to 20%. The region from $y=0$ to $y=5.7$ μm consisted of Al, and the region from $y=5.7$ μm to the upper boundary consisted of CH.

In the code, the material properties, including the resistivity curve, the specific heat capacity curve, and the collisional effect on the fast electrons, i.e. scattering and drag are modeled, are treated in the same way as Davies has previously modeled CH and Al materials [64]. Simulations are run up to 800 fs.

The transverse extent of the coating was taken to cover the entire simulation box. The interface between the metal and the dielectric coating is assumed to be absolutely sharp, in order to take into account the strong adhesion of the coating to the metal substrate. This is the most important feature that, we believe, plays a key role in characterizing the effect of lacquer compared with a standard plastic coating where vacuum gaps may be present which are expected to have a disrupting effect on the fast electron propagation.

Preliminary results of hybrid numerical simulations indicate that the main effect of the rear coating is the suppression of the fine scale filamentation of the fast electron current that is found to occur when the dielectric layer is not present. This suppression is likely to arise from the onset of a large scale quasi-static B-field which is generated at the metal–dielectric interface. The second, important effect shown by the simulations is the build up of a single intense spike of fast electron density that dominates over the plateau. This narrow fast electron bunch will propagate through the target and will likely drive the onset of ion accelerating fields over a much narrower region.

Although additional experimental and modeling work is needed to confirm these results, the scenario is qualitatively consistent with the main effects observed in our experiment, i.e. the suppression of inhomogeneities together with the reduction of the dimensions of the accelerated ion bunch spatial cross-section.

5. Conclusions

In conclusion, production of laser-accelerated proton bunches in the energy range between 1.2 and 3.6 MeV has been achieved with a table-top, 70 fs, 600 mJ Ti:Sa laser. Targets consisting of metal foils either coated with a dielectric layer or uncoated have been used. Our results show that, under our experimental conditions, the employment of a dielectric coating consisting of a layer of lacquer significantly increases the proton bunch spatial cross-section uniformity while reducing its overall transverse dimensions. PIC numerical simulations give proton energies that are consistent with observed values. First results from hybrid simulations suggest that the observed effects may arise from suppression of electron beam filamentation due to a large, quasi-static magnetic field occurring at the metal–dielectric interface.

Acknowledgments

We acknowledge financial support by the MIUR-FIRB project "SPARX" (Sorgente Pulsata Auto-amplificata di Radiazione X), by the MIUR-PRIN-2007 "Studio della generazione di elettroni veloci [...]", by the INFN project PLASMONX and by the HiPER Project [66]. Access to the IOQ installation was supported by LASERLAB. We also wish to acknowledge the ENEA-GRID parallel computer initiative at the Laboratori Nazionali di Frascati, Italy, for the execution of the numerical code calculations, together with the JETI laser crew and the DFG (Deutsche Forschungsgemeinschaft). The present work is part of the "High Field Photonics" CNR Research Unit.

References

[1] K. Krushelnick, Phys. Plasmas 7 (2000) 2055.
[2] S.P. Hatchett, et al., Phys. Plasmas 7 (2000) 2076.
[3] R.A. Snavely, et al., Phys. Rev. Lett. 85 (2000) 2945.
[4] H. Habara, et al., Phys. Rev. E 69 (2004) 036407.
[5] P. McKenna, et al., Phys. Rev. E 70 (2004) 036405.
[6] M. Borghesi, et al., Phys. Plasmas 9 (2002) 2214.
[7] L. Romagnani, et al., Phys. Rev. Lett. 95 (2005) 195001.
[8] F. Cornolti, et al., Phys. Rev. E 71 (2005) 056407.
[9] A.J. Mackinnon, et al., Phys. Rev. Lett. 97 (2006) 045001.
[10] S. Betti, F. Ceccherini, F. Cornolti, F. Pegoraro, Plasma Phys. Contr. Fusion 47 (2005) 521.
[11] F. Ceccherini, S. Betti, F. Cornolti, F. Pegoraro, Laser Phys. 16 (2006) 594.
[12] P. Mora, Phys. Rev. E 72 (2005) 056401.
[13] J. Fuchs, et al., Nature Phys. 2 (2006) 48.
[14] S.V. Bulanov, et al., Phys. Lett. A 299 (2002) 240.
[15] S.V. Bulanov, V.S. Khoroshkov, Plasma. Phys. Rep. 28 (2002) 453.
[16] T.Zh. Esirkepov, et al., Phys. Rev Lett. 89 (2002) 175003.
[17] R. Orecchia, et al., Crit. Rev. Oncol. Hematol. 51 (2004) 81.
[18] A. Brahme, Int. J. Radiat. Oncol. Biol. Phys. 58 (2004) 603.
[19] W.K. Weyrather, J. Debus, Clin. Oncol. 15 (2003) s23.
[20] H. Tsujii, Eur. J. Cancer 37 (2004) s251.
[21] R. Orecchia, et al., Eur. J. Cancer 34 (1998) 459.
[22] U. Amaldi, Analysis 1 (2003) 1.
[23] M. Roth, et al., Phys. Rev. Lett. 86 (2001) 436.
[24] S. Atzeni, J. Meyer-ter-vehn, The Physics of Inertial Confinement Fusion, Beam Plasma Interaction, Hydrodynamics, Hot Dense Matter, Clarendon Press, Oxford, 2004.
[25] M. Borghesi, et al., Phys. Plasmas 9 (2002) 2214.
[26] M. Borghesi, et al., Phys. Rev. Lett. 92 (2004) 055003.
[27] M. Borghesi, et al., Phys. Rev. Lett. 88 (2004) 135002.
[28] T. Cowan, et al., Phys. Rev. Lett. 92 (2004) 204801.
[29] A.J. Kemp, et al., Phys. Rev. E 75 (2007) 056401.
[30] M. Allen, et al., Phys. Rev. Lett. 93 (2004) 265004.
[31] M. Kaluza, et al., Phys. Rev. Lett. 93 (2004) 045003.
[32] T. Ceccotti, et al., Phys. Rev. Lett. 99 (2007) 185002.
[33] H. Schwoerer, et al., Nature (London) 439 (2006) 445.
[34] M. Hegelich, et al., Nature (London) 439 (2006) 441.
[35] S. Ter-Avetisyan, et al., Phys. Rev. Lett. 96 (2006) 145006.
[36] M. Borghesi, et al., Phys. Rev. Lett. 88 (2002) 135002.
[37] M. Schollmeier, et al., Phys. Rev. Lett. 101 (2008) 055004.
[38] A.V. Brantov, V.T. Tikhonchuk, V.Yu. Bychenkov, G. Bochkarev, Phys. Plasmas 16 (2009) 043107.
[39] J. Davis, G.M. Petrov, Phys. Plasmas 16 (2009) 023105.
[40] J. Badziak, et al., Phys. Rev. Lett. 87 (2001) 215001.
[41] H. Kishimura, et al., Appl. Phys. Lett. 85 (2004) 2736.
[42] A. Yogo, et al., Appl. Phys. B 83 (2006) 478.
[43] J. Fuchs, et al., Phys. Rev. Lett. 91 (2003) 255002.
[44] M. Roth, et al., Phys. Rev. ST-AB 5 (2002) 061301.
[45] D. Batani, et al., Plasma Phys. Control. Fusion 48 (2006) B211.
[46] L.A. Gizzi, et al., Phys. Rev. Lett. 76 (1996) 2278.
[47] P. Köster, et al., Plasma Phys. Control. Fusion 51 (2009) 014007.
[48] L.A. Gizzi, et al., Plasma Phys. Control. Fusion 49 (2007) B221.
[49] H. Schwoerer, et al., Phys. Rev. Lett. 96 (2006) 014802.
[50] S. Betti, et al., Phys. Plasmas 16 (2009) 100701.
[51] E. Breschi, et al., Nucl. Instr. and Meth. A 522 (2004) 190.
[52] S. Agostinelli, et al., Nucl. Instr. and Meth. A 506 (2003) 250.
[53] D. Giulietti, et al., Phys. Plasmas 9 (2002) 3655.
[54] A. Giulietti, et al., Phys. Rev. Lett. 101 (2008) 105002.
[55] J.F. Ziegler, et al., SRIM—The Stopping and Range of Ions in Matter, SRIM Co., 2008, ISBN 0-9654207-1-X. Numerical code freely available online at ⟨http://www.srim.org⟩.
[56] S. Betti, et al., Laser accelerated proton yield control via rear-surface target coating, Technical Report No. 01/2008 (prot. 206 of 30/01/2008), ILIL-IPCF, CNR, Pisa, Italy (unpublished). Freely available online at ⟨http://ilil.ipcf.cnr.it⟩.
[57] H. Alfven, Phys. Rev. E 55 (1939) 425.
[58] A.R. Bell, J.R. Davies, S. Guerin, H. Ruhl, Plasma Phys. Controll. Fusion 39 (1997) 653.
[59] F. Pisani, Phys. Rev. E 62 (2000) R5927.
[60] D. Batani, Phys. Rev. Lett. 94 (2005) 055004.
[61] Y.T. Li, Phys. Rev. E 72 (2005) 066404.
[62] A.P.L. Robinson, M. Sherlock, Phys. Plasmas 14 (2007) 083105.
[63] A.R. Bell, et al., Plasma Phys. Control. Fusion 48 (2006) R37.
[64] J.R. Davies, Phys. Rev. E 65 (2002) 026407.
[65] A.P.L. Robinson, Phys. Rev. Lett. 100 (2008) 025002.
[66] ⟨http://www.hiper-laser.org⟩.